Polyfunctional Methodology for Improved DFT Thermochemical Predictions

Anne Marie Shough, Douglas J. Doren, and Dominic M. Di Toro*

Department of Chemistry and Biochemistry and Department of Civil and Environmental Engineering, University of Delaware, Newark, Delaware 19716

Received: May 30, 2008; Revised Manuscript Received: July 29, 2008

Statistical error distributions for enthalpies of formation as predicted by 18 different density functionals have been analyzed using a test set of 675 molecules. Systematic errors, dependent on the number of valence electrons, have been identified for some functionals. A simple empirical correction makes a significant improvement in the prediction error for these single functionals. Linear combinations of enthalpy estimates from different density functionals are identified that exploit the error correlations among the functionals and allow for further improvements in the accuracy of thermodynamic predictions. A good compromise between accuracy and computational efforts is achieved by the BLUE (best linear unbiased estimator) combination of three functionals, B3LYP, BLYP, and VSXC (polyfunctional 3 or PF3). The PF3 method has a mean absolute deviation (MAD) from experiment of 2.4 kcal/mol on the G3 set of 271 molecules. This can be compared to the MAD of 4.9 kcal/mol for B3LYP and 1.2 kcal/mol for the more costly G3 method. On the larger set of 675 molecules, the MAD for PF3 is 3.0 kcal/mol. Opportunities for further improvements in the accuracy of this method are discussed.

1. Introduction

In recent decades, significant strides have been made in molecular electronic structure theory, allowing for the prediction of thermochemical data to chemical accuracy. This has been a result not only of advances in methodology but also computational technology. In general, coupled-cluster (CC) theory[1−5] achieves the highest accuracy[6,7] while bearing the highest computational cost. Both the Weizmann-*n* (W*n*) methods[8−11] and HEAT methods[12] combine CC theory with extrapolation schemes and additional corrections to improve the prediction of thermochemical data with mean absolute deviations (MAD) of ∼0.3 kcal/mol. However, these methods are practical for only small molecules. Much less costly are the Gaussian-*n* (G*n*)[13−20] methods, based on a combination of empirical corrections and additive approximations applied to lower level calculations, and the complete basis set (CBS) methods,[21−26] involving extrapolation schemes. These methods yield MAD values of ∼1 kcal/mol. Currently, it is rare for G*n* methods to be applied to systems having more than 10−12 heavy atoms.

For larger systems, density functional theory (DFT) is generally employed, but even for the best, functionals achieve lower accuracy, with MAD values ∼3.5−4.5 kcal/mol.[19,27] Many studies have been carried out to identify and compare the errors for various combinations of exchange and correlation functionals.[27−32] A variety of approaches have also been taken to remove the deficiencies in current density functionals. For example, kinetic energy density terms[33] and self-interaction corrections[34] have been included. Functionals have been developed based entirely on requirements from first-principles,[35] while others are parametrized to fit empirical data.[36] Post hoc corrections may also be applied to improve the accuracy of predicted thermochemical properties.[32,37] For example, Friesner et al.[32] have identified systematic errors in B3LYP related to the bonding environment that may be improved upon using simple empirical corrections.

In this paper, we identify systematic errors in some functionals that depend on the number of valence electrons in the system. Accounting for these errors post hoc can lead to significant improvement in individual functional performance. There is also a high degree of correlation between the residuals of different functionals. We have identified linear combinations of individual, self-consistent density functional estimates that exploit these correlations by allowing for a cancelation of errors. This improves the prediction accuracy for enthalpies of formation (MAD ∼ 2.4 kcal/mol) with relatively little additional effort. We refer to this approach as the polyfunctional (PF) method. In some ways this is similar to the G*n* methods[13−20] and the multicoefficient correlation methods (MCCM) of Truhlar et al.[38−45] in that it combines results from several independent calculations. The G*n* methods combine a set of lower-level calculations, each with a coefficient of one, to estimate the predictions of a high level of theory. The MCCM combinations use nonunity coefficients determined by fits to experimental data. Similar to MCCM, the PF method combines weighted energies from multiple independent calculations. In contrast to Gn and MCCM, the PF method uses only DFT calculations, rather than more costly MP*n*, CCSD, or QCISD calculations. The polyfunctional approach makes no a priori assumptions about which combinations of methods will allow error cancelation.

Note that the PF approach is fundamentally different from an improved density functional that combines various exchange and correlation functionals in a single self-consistent calculation. However, the results reported here do suggest that there is substantial room for systematic improvement in standard classes of density functionals. In the absence of fundamental advances, the empirical approach taken here offers a rapid, practical approach to improved predictions.

* Corresponding author. Tel: 302 831 4092. Fax: 302 831 3640. E-mail: dditoro@udel.edu.

10.1021/jp804784s CCC: $40.75
Published on Web 09/30/2008

2. Data Sets and Methods

A data set including empirical thermochemical data for 675 molecules has been used as a standard for comparing the predictions of different functionals. The data set comprises the 271 molecules used for enthalpy of formation and atomization energy analysis in the G3 data set as well as 404 additional first- and second-row molecules. All experimental values were taken from the National Institute of Standards and Technology Chemistry Webbook.[46] While the set of 404 molecules has a wider range of experimental error than the 271 molecules used for G3 analysis, we have included them to increase the number of data that are available. This increases the reliability of the statistical estimates, so long as there is no systematic error in the non-G3 molecules. We will address this issue below.

All calculations have been carried out using the Gaussian 03 program.[47] Each molecular geometry was optimized using Becke's three-parameter hybrid functional,[36] B3LYP, with a 6-31G* basis set. Thermodynamic corrections were determined using the same model chemistry with a 0.96 scaling factor. This is the same method employed in the G3//B3LYP and G3(MP2)//B3LYP variations of G3 for determination of optimized geometries and thermodynamic corrections.[16] Electronic energies for each molecule were calculated using a 6−311++G(3df,2p) basis set for each of the following 18 functionals: B3LYP,[36] B3PW91,[36,48−50] B98,[51,52] B972,[53] BLYP,[54−56] BP86,[54,57] BPW91,[48−50,54] BVWN5,[54,58] HCTH,[59] MPW1PW91,[48−50,60] OLYP,[55,56,61] OP86,[57,61] OPBE,[35,61,62] OPW91,[48−50,61] OVWN5,[58,61] PBE,[35,62] PBE0,[35] VSXC.[33]

The enthalpies of formation at 298 K for each molecule are calculated as follows. The enthalpy of formation at 0 K is

$$\Delta_f H^\circ(M, 0\mathrm{K}) = \varepsilon_0(M) + \sum_{\text{atoms}} x(\Delta_f H^\circ(X, 0\mathrm{K}) - \varepsilon_0(X)) \quad (1)$$

where x is the number of atoms of element X in molecule M, $\Delta_f H°(X,0\mathrm{K})$ are the experimental atomic enthalpies of formation at 0 K taken from ref 63, and ε_0 are the calculated electronic energies for the atoms X and the molecule M, including the molecular zero-point energy correction, for a given functional. To estimate the enthalpy of formation at 298 K, $\Delta_f H°(M,298\mathrm{K})$, the calculated enthalpy corrections for the molecule, $\Delta H_M^\circ(298\mathrm{K}-0\mathrm{K})$, and the experimental enthalpy corrections for the atoms, $\Delta H_X^\circ(298\mathrm{K}-0\mathrm{K})$ (taken from ref 63), are included to yield

$$\Delta_f H^\circ(M, 298\mathrm{K}) = \Delta_f H^\circ(M, 0\mathrm{K}) + \Delta H_M^\circ(298\mathrm{K} - 0\mathrm{K}) - \sum_{\text{atoms}} x(\Delta H_X^\circ(298\mathrm{K} - 0\mathrm{K})) \quad (2)$$

The experimental enthalpies for some of the third-row molecules in the data set require theoretical input. In accord with Curtiss et al.,[19] the atomization energies for these molecules are used in place of the enthalpy values and are evaluated using

$$\sum D_0(M) = \sum_{\text{atoms}} x\varepsilon_0(X) - \varepsilon_0(M) - \varepsilon_{\mathrm{ZPE}}(M) \quad (3)$$

where $\sum D_0(M)$ is the atomization for the molecule, M, $\varepsilon_{\mathrm{ZPE}}(M)$ is the zero-point correction for the molecule, and x, X and ε_0 are defined above.

The *R* statistical environment[64] has been used for all subsequent statistical analyses.

3. Results and Discussion

3.1. Individual Functional Performance. Figure 1 presents box and whiskers plots[65] of the residuals (*experimental-predicted* enthalpies) for each of the 18 functionals. The median (dark bar), the 75th−25th percentile range (the box), the approximate 5−95% confidence limits (the whiskers each having a range of 1.5 times the width of the box), and the values outside the confidence limits (circles) are shown. Note the scale changes for the two panels. It is clear that the functionals have a wide range of accuracies, but even the best functionals have interquartile ranges (IQR, 75th−25th percentile) on the order of 6−6.5 kcal/mol. The majority of these functionals also have a positive or negative bias that can be quite severe, for example, the functionals with P86 and VWN5 correlation.

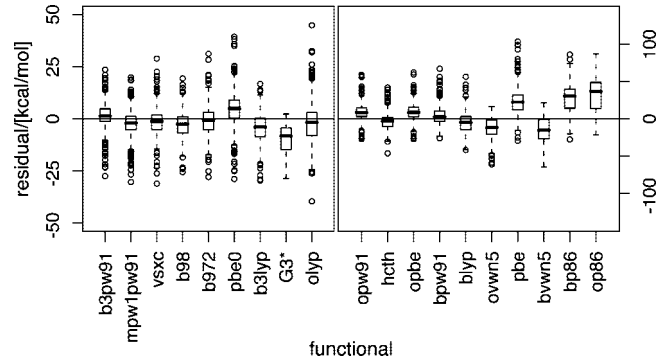

Figure 1. Box and whiskers plot comparing the residuals for all 18 functionals and the G3* residuals (G3 residuals where the HLC has been removed). The functionals are ordered by IQR values (left to right) and have been divided into two panels having different *y*-axis scales to highlight the range of performance for all of the methods. The median (dark bar), the 75th−25th percentiles (the box), the approximate 5−95% confidence limits (the whiskers), and the values outside the confidence limits (circles) are shown.

The G*n* methods[13−20] account for a systematic error in the electronic energy that increases with the number of electrons in the system. This bias is corrected using higher-level corrections (HLC) to the electronic energies for the molecule, $\Delta E_M(\mathrm{HLC})$, and atoms, $\Delta E_X(\mathrm{HLC})$. In G3 the corrections in kcal/mol are[16]

$$\Delta E_M(\mathrm{HLC}) = 4.007 n_\beta + 1.868(n_\alpha - n_\beta) \quad (4)$$

$$\Delta E_X(\mathrm{HLC}) = 3.902 n_\beta + 1.161(n_\alpha - n_\beta) \quad (5)$$

where n_α and n_β are the number of α and β valence electrons, respectively. To visualize the magnitude of this correction, the HLC terms are removed from the G3 residuals and shown as G3* in Figure 1. Without the HLC term, G3 has a negative bias and an IQR ∼ 10 kcal/mol.

Many of the functionals studied here also show a strong dependence of residual on the number of electrons in the system. Figure 2 shows the relationship between the residuals and the total number of valence electrons in the molecule, $n_\alpha + n_\beta$, for selected functionals. While the residuals for some functionals have no systematic dependence on $n_\alpha + n_\beta$ (e.g., VSXC), other functionals have a strong positive (e.g., PBE) or negative (e.g., BVWN5) bias. To remove this bias, we have estimated a HLC for each functional i by fitting the enthalpy residuals to a linear equation with n_β and $n_\alpha - n_\beta$ as the independent variables, i.e.

$$\Delta E(\mathrm{HLC})_i = b_{0,i} + b_{1,i} n_\beta + b_{2,i}(n_\alpha - n_\beta) \quad (6)$$

This term was then subtracted from the residuals for each functional i. The coefficients for the $\Delta E(\mathrm{HLC})_i$ of each functional can be found in Table S1 of the Supporting Information. Note that this HLC includes a constant term that is not present in the G3 HLC. The $b_{0,i}$ terms guarantee that the average error for each functional is zero. Figure 3 illustrates

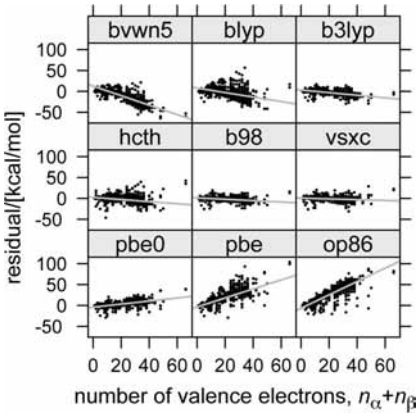

Figure 2. Scatter plots illustrating the relationship between the residual errors and the total number of valence electrons for selected functionals. Gray regression lines had been added to facilitate the visualization of the bias.

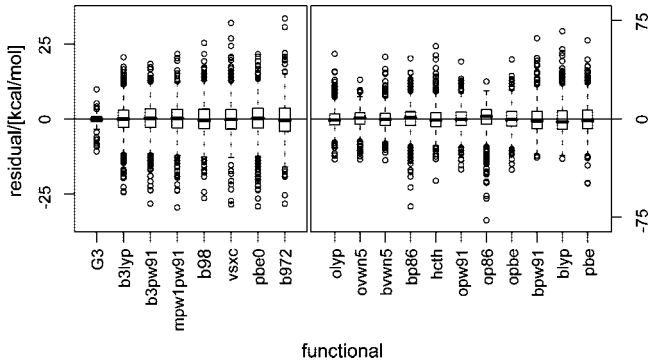

Figure 3. Box and whiskers plot comparing the residuals for all 18 functionals and the G3 residuals *after* the HLC terms have been applied. The functionals are ordered by IQR values (left to right) and have been divided into two panels having different *y*-axis scales to highlight the range of performance for all of the methods.

the improvement in the functional performance after applying the HLC terms (note scale changes in the two panels relative to Figure 1). The residual distributions are now all centered at or near 0, with a significant reduction in the IQR for all functionals. G3 now has the smallest IQR (1.7 kcal/mol) followed by B3LYP (5.78 kcal/mol) and the other functionals.

Several functionals used in this study make use of the same (or similar) correlation functional (e.g., OP86/BP86, OPW91/BPW91) or the same (or similar) exchange functional (e.g., BLYP/BVWN5, OPBE/OLYP). Additionally, some of these functionals are closely related. For example, B98 and B972 are both modified versions of the B97 functional. Therefore, the errors for many functionals are strongly correlated. The lower triangle of Figure 4 presents cross correlation plots of the standardized residuals

$$Z\{e_i(M_k)\} = \frac{e_i(M_k) - \bar{e}_i}{\sigma_i} \tag{7}$$

where $e_i(M_k)$ is the residual (experimental-predicted)

$$e_i(M_k) = H(M_k) - H_i(M_k) \tag{8}$$

for a given functional i and molecule M_k, and $\bar{e}_i$ and σ_i are the mean and standard deviations of the residuals, respectively, for a given functional i. Each panel below the diagonal shows a scatterplot of the standardized residual of the functional listed in the column versus the functional listed in the row. The correlation coefficients are given in the upper triangle following

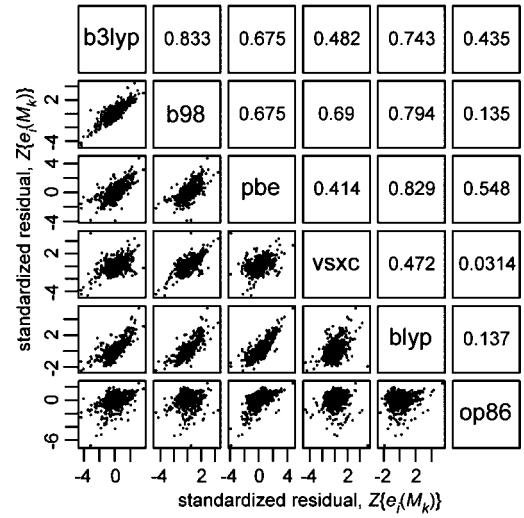

Figure 4. Pairs plot presenting the correlation between the residual errors of selected functionals. Displayed in the lower left panels are crossplots for the standardized error (eq 7) of the functional at the head of the column diagonal versus the functional listed in the row. Note that the scales for each of the standardized scatterplots are slightly different. The correlation coefficient for each functional pair is also listed in the upper right panels following the same convention.

the same convention. The correlation coefficients for the full set of 18 functionals are provided in Table S2 of the Supporting Information. As we will show, these correlations can be exploited by combining the estimates from selected functionals to produce an improved estimate for thermochemical data, referred to as the PF method.

3.2. BLUE. We will use a linear combination of the enthalpies of formation estimated with a number of functionals as an improved estimate of the actual enthalpy of formation. For a given set of functionals, the best linear unbiased estimator (BLUE) method[66] is used to determine the coefficients of the linear combination. It is also possible to use linear regression (LR) to estimate the coefficients. The difference between the two methods is in the description of the error structure. In LR, all of the predictors (the various functional estimates) are assumed to be known with no error. The error is included as an additional term in the linear equation that relates the actual enthalpy of formation to the functional estimates. In the BLUE formulation, it is assumed that there is a true but unknown value of the enthalpy of formation and we have multiple "observations", the results of the various functionals. These observations are corrupted by errors that are treated as random errors with zero means and known covariance matrix. The reason we use the BLUE formulation is that it more exactly mirrors the idea that each functional estimate is an approximation to the exact enthalpy and that the errors made by the various functionals can be modeled as random errors that are correlated. Using this framework, the prediction error expected from the BLUE method can be calculated. In LR, the error is assumed to be independent from molecule to molecule and to have constant variance and no correlation between molecules. This appears to be a less appropriate model for the problem at hand. The errors are associated with the performance of the functionals (BLUE) rather than a random error associated with each molecule (LR).

3.2.1. Two Functional Estimate. To clarify the basis for the method and to illustrate when it will be effective, the BLUE equations are first derived for a PF estimate using two functionals, H_1 and H_2. For a given molecule M_k, the true enthalpy is denoted by $H(M_k)$. The predicted enthalpies for each

functional are denoted as $H_1(M_k)$ and $H_2(M_k)$. For each functional it is assumed that the probability distributions of the residuals e_1 and e_2 (eq 8) have zero means. This is the reason that the bias with respect to electron number has been removed for each functional (eq 6). No distributional assumption is made, e.g., e_i are not required to be normal random variables. The only assumption is that the optimal estimate, $\hat{H}(M_k)$, of $H(M_k)$ is linear in the "observations" $H_1(M_k)$ and $H_2(M_k)$, i.e.

$$\widehat{H}(M_k) = w_1 H_1(M_k) + w_2 H_2(M_k) \tag{9}$$

where w_1 and w_2 are the weights for the observations H_1 and H_2, respectively.

Two conditions are needed to determine the weights w_1 and w_2. The first is that the optimal estimate, $\hat{H}(M_k)$, is unbiased., i.e.

$$E\{\hat{e}\} = E\{\widehat{H}(M_k) - H(M_k)\} = E\{w_1 H_1(M_k) + w_2 H_2(M_k) - H(M_k)\} = 0 \tag{10}$$

where $E\{\hat{e}\}$ is the average (mean) of the residuals $\hat{e} = \hat{H}(M_k) - H(M_k)$ over all M_k molecules and eq 9 has been substituted for $\hat{H}(M_k)$. Note that if

$$1 = w_1 + w_2 \tag{11}$$

then eq 10 is satisfied since

$$E\{e_i(M_k)\} = E\{H(M_k) - H_i(M_k)\} = E\{w_i H(M_k) - w_i H_i(M_k)\} = 0 \tag{12}$$

for both H_1 and H_2.

The second condition is that the w_i minimize the variance of $\hat{e}$, the residuals of $\hat{H}$

$$V\{\hat{e}\} = V\{w_1 e_1 + w_2 e_2\} = {w_1}^2{\sigma_1}^2 + {w_2}^2{\sigma_2}^2 + 2w_1 w_2 \sigma_1 \sigma_2 \rho \tag{13}$$

where e_1 and e_2 are the residuals from $H_1(M_k)$ and $H_2(M_k)$ (eq 8), ${\sigma_1}^2$ and ${\sigma_2}^2$ are the variances of e_1 and e_2, and ρ is the correlation coefficient between e_1 and e_2. Substituting eq 11 into eq 13 yields

$$V\{\hat{e}\} = {w_1}^2{\sigma_1}^2 + (1 - w_1)^2{\sigma_2}^2 + 2w_1(1 - w_1)\sigma_1\sigma_2\rho \tag{14}$$

The minimum variance is found by requiring that

$$\frac{\partial V\{\hat{e}\}}{\partial w_1} = 0 \tag{15}$$

or

$$w_1 = \frac{\sigma_1\sigma_2\rho - {\sigma_2}^2}{2\sigma_1\sigma_2\rho - {\sigma_1}^2 - {\sigma_2}^2} \tag{16}$$

This can be simplified by defining the ratio r of the standard deviation of residual e_1 to that of e_2

$$r = \frac{\sigma_2}{\sigma_1} \tag{17}$$

to yield

$$w_1 = \frac{r(\rho - r)}{2r\rho - r^2 - 1} \tag{18}$$

In the limit of large r (e_2 has a much larger standard deviation than e_1), $w_1 \rightarrow 1$, so $\hat{H} = H_1$ and H_2 does not contribute to the optimal estimate. To illustrate how $V\{\hat{e}\}$ varies with r, the variance of residuals (eq 14) is normalized with respect to ${\sigma_1}^2$

$$\frac{V\{\hat{e}\}}{{\sigma_1}^2} = \frac{r^2(\rho^2 - 1)}{2r\rho - r^2 - 1} \tag{19}$$

This normalized variance is the factor by which the residual variance is reduced when using the two-functional linear estimation $\hat{H}(M_k)$ (eq 9) to estimate $H(M_k)$, instead of the single functional $H_1(M_k)$. Figure 5 presents $V\{\hat{e}\}/{\sigma_1}^2$ and w_1 versus r for various values of ρ.

The top and bottom panels of each graph are for positive ($\rho \geq 0$) and negative ($\rho < 0$) residual correlation, respectively.

Considering first the case for negatively correlated residuals (bottom panels of Figure 5), $V\{\hat{e}\}/{\sigma_1}^2$ decreases (the estimate improves) with increasing negative correlation, as $\rho \rightarrow -1$. However $V\{\hat{e}\}/{\sigma_1}^2$ increases with increasing r. The lowest value of $V\{\hat{e}\}/{\sigma_1}^2$ is obtained for two functionals having strong negative error correlation and the same error variances, $r = 1$. For this case ($r \rightarrow 1$, $\rho \rightarrow -1$), the errors in the two functionals have the same magnitude but opposite sign, so almost complete cancelation of error can be achieved. The weight w_1 for H_1 (right graph), is always less than 1 when e_1 and e_2 are negatively correlated. Because the two weights must sum to 1 (eq 11), the weights will both be positive. As σ_2 becomes larger than σ_1

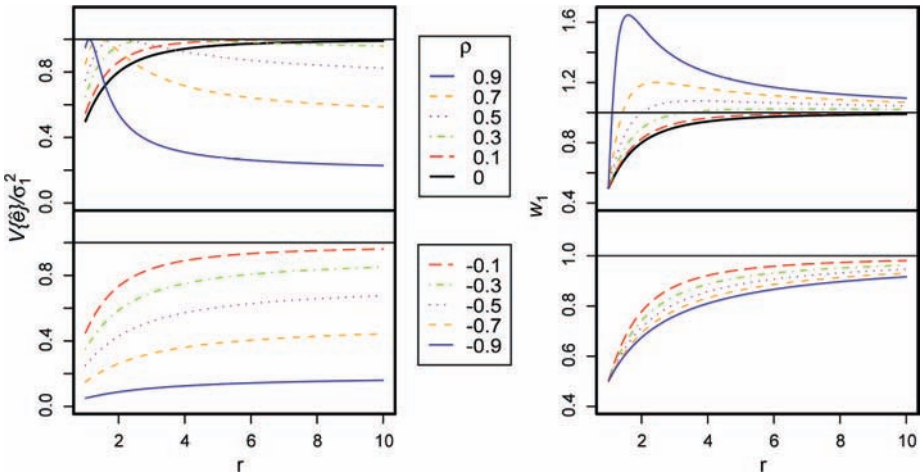

Figure 5. The effect of the BLUE parameters r and ρ on $V\{\hat{e}\}/{\sigma_1}^2$ (left) and w_i (right) for $N_f = 2$ as derived in eqs 19 and 18. Positive and negative values of ρ are separated into top and bottom portions of each graph, respectively. A heavy, black line is used to distinguish $\rho_{i,j} = 0$ in the top plots.

($r > 1$), H_2 contributes less and less to the overall value of $\hat{H}$ and $V\{\hat{e}\}/\sigma_1^2 \rightarrow 1$ (no improvement over H_1).

In the present study, there are no negative correlations between the residuals of the 18 functionals after removing the bias due to electron number (Figure 4 and Table S2 of the Supporting Information). Therefore, only the cases with positive ρ (top panels of Figure 5) apply. For low positive error correlation, $\rho \leq 0.5$, $V\{\hat{e}\}/\sigma_1^2$ increases monotonically with increasing r, similar to the negatively correlated cases, but with significantly higher values of $V\{\hat{e}\}/\sigma_1^2$.

In contrast, for variables having strong positive error correlation, $\rho > 0.5$, $V\{\hat{e}\}/\sigma_1^2$ first increases with r and then, surprisingly, decreases. That is, a large enough difference in the standard deviation of the two functional errors can be exploited to reduce the error of the optimal estimate. This result can be understood by examining w_1 for $\rho = 0.9$. For $r > 1/0.9$, w_1 is greater than unity and therefore w_2 is negative. Thus $\hat{H}$ is a weighted *difference* between H_1 and H_2. Note that as r increases $V\{\hat{e}\}/\sigma_1^2$ continues to decrease, indicating that a more accurate estimate can be achieved. This is possible because the errors made by H_1 and H_2 are strongly correlated and in the same direction. If $r \gg 1$, then the H_2 error is much larger than that of H_1, so scaling it down (small w_2) and subtracting it (negative w_2) cancels part of the error in H_1 and reduces the error in $\hat{H}$. If $r = 1$, then they are both of similar magnitude and nothing can be done, i.e., $V\{\hat{e}\}/\sigma_1^2 = 1$.

3.2.2. Polyfunctional Estimate. When N_f functionals are used in a linear estimator, the optimal estimate is[66]

$$\hat{H} = \sum_{i=1}^{N_f} w_i H_i = \mathbf{w}^T \mathbf{H} \tag{20}$$

where the weights, w_i, are the elements of the column vector

$$\mathbf{w} = \frac{\mathbf{\Sigma}^{-1}\mathbf{1}}{\mathbf{1}^T\mathbf{\Sigma}^{-1}\mathbf{1}} \tag{21}$$

H is the column vector of unbiased enthalpy estimates from the various functionals, $\mathbf{H} = [H_1, H_2, ..., H_{N_f}]^T$, $\mathbf{\Sigma}$ is the covariance matrix of the unbiased functional errors with elements

$$\Sigma_{ij} = [\sigma_i \sigma_j \rho_{ij}] \tag{22}$$

where σ_i^2 is the variance of e_i, ρ_{ij} is the correlation coefficient for e_i and e_j of functionals H_i and H_j, respectively, and $\mathbf{1} = [1, 1, ..., 1]^T$ is the column vector of ones. The variance in the error of the optimal estimate, $\hat{e}$, is

$$V_{BLUE}\{\hat{e}\} = \frac{1}{\mathbf{1}^T\mathbf{\Sigma}^{-1}\mathbf{1}} \tag{23}$$

The unbiased estimates H_i are obtained from the enthalpy estimates, $\Delta_f H_i^\circ$ (eq 2), by using the higher level correction (eq 6)

$$\begin{aligned} H_i &= \Delta_f H_i^\circ + \Delta E(\mathrm{HLC})_i \\ &= \Delta_f H_i^\circ + (b_{0,i} + b_{1,i}(n_\beta) + b_{2,i}(n_\alpha - n_\beta)) \end{aligned} \tag{24}$$

Therefore,

$$\hat{H} = \sum_i w_i \Delta_f H_i^\circ + a_0 + a_1(n_\beta) + a_2(n_\alpha - n_\beta) \tag{25}$$

where

$$a_j = \sum_i w_i b_{j,i} \tag{26}$$

for $j = 0, 1, 2$.

3.3. Identification of Optimal Polyfunctional Combinations. The BLUE equations provide the optimal estimate for a given set of functionals. However, a method is required to identify the best choice of functionals to include in the PF estimate. To identify the optimal PF combination for a given *number* of functionals (N_f) an exhaustive search is performed among all combinations of N_f functionals chosen from the full set of 18 functionals (262 143 total combinations). For each combination, the BLUE weights were determined (eq 21) using the set of 675 molecules. These weights were then used to predict optimal estimates (eq 25) for the enthalpies of formation for the entire molecule set. For $N_f = 1-9$, the five functional combinations with the lowest RMSEP (root mean squared error of prediction) are illustrated in Figure 6. Optimal combinations of $N_f = 2$ or 3 significantly reduce the RMSEP relative to that of a single functional. Additionally, for $N_f = 1$, 2, or 3, there is a significant difference in RMSEP between the first- and fifth-ranked PF combination. Beyond $N_f = 3$, however, there is little change between the first- and fifth-ranked PF combination for a given N_f, so multiple PF combinations produce similar results. Figure 6 also shows that there is no significant reduction in the RMSEP beyond $N_f = 5$.

3.4. Best Polyfunctional Estimates. The weights corresponding to the best PF combinations for $N_f = 1-5$ are shown in Figure 7. The best individual functional in this set, denoted PF1, is the commonly used B3LYP functional. By including the HLC term, the RMSEP for B3LYP is decreased from 7.88 to 5.46 kcal/mol, resulting in a significant improvement in accuracy.

On the basis of the analysis in section 3.2.1, the best $N_f = 2$ combinations for the 18 functional set will include functionals having strong positive error correlation (high ρ) and significantly different error distributions (high r). The σ_i values for some selected functionals are on the diagonal (bolded) of Table 1. These functionals are listed in order of increasing σ, left to right (*or* top to bottom). Table 1 also presents the values of ρ (upper right triangle, italicized) and $\sqrt{V\{\hat{e}\}}$ (lower left triangle) for each functional pair in the corresponding column and row. The optimal functional pairs would therefore include one functional from the far left and one functional from the far right (to have significantly different values of σ, and thus a high r) as well as a high value of ρ. Two such functional pairs have been marked in Table 1, B98:BLYP and B3LYP:BLYP. For both functional

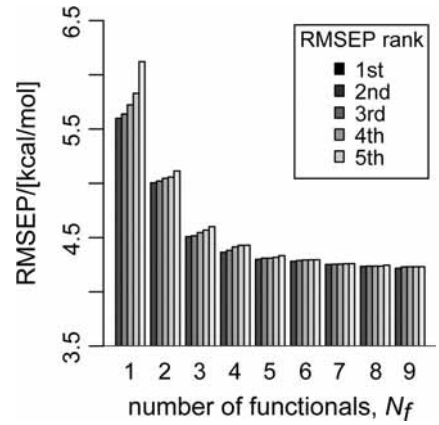

Figure 6. Bar plot comparing the RMSEP of the five best functional combinations for $N_f = 1-9$.

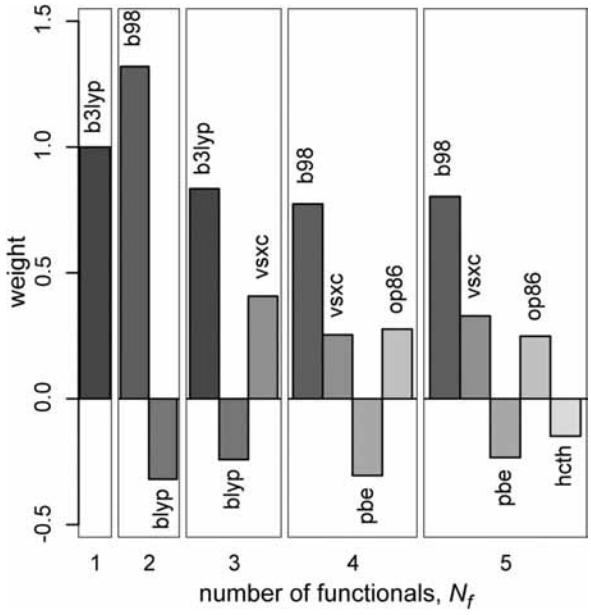

Figure 7. BLUE functional weights for the best PF combinations $N_f = 1-5$.

TABLE 1: BLUE Parameters for Selected Functionals Pairs[a,b]

	B3LYP	B98	VSXC	HCTH	OP86	BLYP	PBE
B3LYP	**5.60***	*0.833*	*0.483*	*0.590*	*0.435*	*0.743†*	*0.675*
B98	5.42	**5.73***	*0.689*	*0.775*	*0.135*	*0.794‡*	*0.675*
VSXC	5.02	5.42	**6.13**	*0.696*	*0.0314*	*0.472*	*0.414*
HCTH	5.60	5.45	6.08	**10.0**	*0.178*	*0.768*	*0.726*
OP86	5.59	5.37	5.46	8.14	**11.4**	*0.137*	*0.548*
BLYP	5.13†	5.01‡	6.12	10.0	8.96	**12.5***	*0.829*
PBE	5.35	5.49	6.11	9.97	10.5	12.0	**12.6**

[a] The diagonal (**bold**) contains the value of σ for each individual functional. The lower left and upper right (*italic*) contain the predicted $\sqrt{V\{\hat{e}\}}$ and the correlation coefficient, ρ, respectively, for the corresponding functional pairs in the column and row. [b] Denoted by *, †, and ‡ are the B3LYP:BLYP pair and B98:BLYP pair having large ρ and r values resulting in small values of $\sqrt{V\{\hat{e}\}}$ and thus are the optimal $N_f = 2$ functional pairs combinations.

pairs, $\rho_{ij} > 0.7$ and $r > 2$, resulting in the low values of $\sqrt{V\{\hat{e}\}}$ (~5 kcal/mol). The best combination of two functionals found in our exhaustive search, PF2, uses B98 and BLYP (Figure 7), though several other combinations have similar RMSEP values (Figure 6).

The same types of relationships determine the best polyfunctional combinations with $N_f > 2$. For example, B3LYP and BLYP are both present in the best PF3 combination along with VSXC (Figure 7). Above $N_f = 3$, B98, instead of B3LYP, is identified as the leading contributor to the best PF combination (Figure 7). However, there exists a B3LYP combination for each N_f that yields comparable RMSEP values to an analogous B98 combination. This is due to the strong correlation and similar error variances for the B3LYP and B98 functionals (Table 1).

Figure 7 shows that many of the same functionals are used repeatedly in the best PF combinations. For example, the VSXC functional is employed in PF3−5 and has been identified in most of the best, high-order PF combinations. The VSXC functional includes terms dependent on the noninteracting kinetic energy density that are not found in the description of most other density functionals. This allows for a more flexible form of the exchange-correlation functional, leading to a relatively high prediction accuracy for thermochemical estimates (Table 1 and Table S2 of the Supporting Information). The VSXC functional is also one of the few functionals where the errors in the enthalpy estimates are independent of the total number of valence electrons (Figure 2).

The BLYP functional is also repeatedly used in the best PF combinations (PF2−5). The BLYP and B3LYP functionals differ primarily in the inclusion of exact Hartree−Fock (HF) exchange in the B3LYP functional. At first glance, the combination of both the B3LYP and BLYP functionals in PF3 suggests a partial cancellation of the BLYP portion of the B3LYP estimate and thus a higher relative contribution of exact exchange. However, the estimation made by weighting the results of B3LYP and BLYP calculations is very different from the estimation made by changing the weight of HF exchange in B3LYP. In the latter case, a single self-consistent calculation is carried out with a modified functional. In the PF method, independent self-consistent calculations are carried out with different functionals, leading to multiple approximations to the density. The resulting estimates of the energy are then weighted and combined, resulting in a cancellation of errors and an improved estimate.

The functionals involved in the best PF combinations may suggest useful combinations of properties to include in the development of future, more accurate, density functionals. However, a single self-consistent calculation involving a weighted combination of the exchange and correlation functionals of a given PF*n* combination will not result in the same estimate determined by the PF*n* method.

The final functional weights and HLC parameters for the PF1 to PF5 combinations are listed in Table 2. These coefficients are identified as "BLUE full", as the fits were made using the full data set. The other set of coefficients included in Table 2 will be discussed below. An example calculation of the complete PF3 method for isobutene has been included in Scheme S1 of the Supporting Information to facilitate the implementation of the PF methodology.

3.5. Cross-Validation and Sensitivity to Training Set. Cross-validation has been employed to test the robustness of the PF combinations. From the entire data set, 25% of the molecules were randomly set aside to serve as a validation set. The remaining 75% of the molecules were used as the training set to calculate optimal coefficients using the BLUE method. These coefficients were then used to predict the enthalpies of formation. The RMSEP values for both the training and validation sets were computed. This process was repeated for a total of 50 cross-validation realizations. The mean and standard deviations of the training and validation RMSEP are presented in Figure 8 for $N_f = 1-5$. The averaged RMSEP values are almost identical for the training and validation sets at each N_f, indicating that the BLUE estimates perform well for the molecules not used to estimate the optimal weights. The variations in RMSEP, indicated by the ±2 standard deviation bars, show that the estimation error is not largely influenced by the chosen subsets for either the training (range in RMSEP ~ 0.5 kcal/mol) or validation (range in RMSEP ~ 1.5 kcal/mol) sets. Therefore, the BLUE estimates are robust and do not suffer from fluctuations due to a specific set of molecules included in the estimation training set. This is in part due to the large number of molecules (75% of 675) used to make the estimate.

3.6. Analysis of Predictability. Probability plots[67] of the residual errors have been used to assess the predictive capabilities of the PF combinations (Figures 9 and 10). In these figures, a residual of 3 kcal/mol plotted at a 0.95 probability implies that 95% of the molecules in the distribution have a residual ≤3 kcal/mol. The points of the probability plot will lie on a

TABLE 2: Coefficients, Weights, Standard Deviations, and $\sqrt{V\{\hat{e}\}}$ Values As Determined by the Full BLUE and Bootstrapped BLUE Methods for the Best PF1−PF5 Combinations[a]

	PF1						
	B3LYP	a_0[b]	a_1[c]	a_2[d]	$\sqrt{V_{\mathrm{BLUE}}\{\hat{e}\}}$	$\sqrt{V^{\mathrm{coef}}_{\mathrm{BLUE}}\{\hat{e}\}}$	$\sqrt{V\{\hat{e}\}}$
BLUE full	1.0000	2.755	−0.5929	0.4170	5.603		
BLUE bootstrap	1.0000	2.769	−0.5931	0.4210	5.594	0.3859	5.603
SD bootstrap	0.0000	0.5998	0.4579	0.5227			

	PF2							
	B98	BLYP	a_0[b]	a_1[c]	a_2[d]	$\sqrt{V_{\mathrm{BLUE}}\{\hat{e}\}}$	$\sqrt{V^{\mathrm{coef}}_{\mathrm{BLUE}}\{\hat{e}\}}$	$\sqrt{V\{\hat{e}\}}$
BLUE full	1.320	−0.3195	−1.464	−0.04996	1.100	5.009		
BLUE bootstrap	1.320	−0.3197	−1.440	−0.05096	1.088	4.986	0.4438	5.009
SD bootstrap	0.02610	0.02610	0.6829	0.05571	0.5004			

	PF3								
	B3LYP	BLYP	VSXC	a_0[b]	a_1[c]	a_2[d]	$\sqrt{V_{\mathrm{BLUE}}\{\hat{e}\}}$	$\sqrt{V^{\mathrm{coef}}_{\mathrm{BLUE}}\{\hat{e}\}}$	$\sqrt{V\{\hat{e}\}}$
BLUE full	0.8342	−0.2415	0.4073	0.3657	−0.2891	1.034	4.512		
BLUE bootstrap	**0.8348**	**−0.2416**	**0.4068**	**0.3863**	**−0.2901**	**1.030**	4.490	0.4282	4.512
SD bootstrap	0.04304	0.02299	0.03077	0.5290	0.04098	0.4378			

	PF4									
	B98	VSXC	PBE	OP86	a_0[b]	a_1[c]	a_2[d]	$\sqrt{V_{\mathrm{BLUE}}\{\hat{e}\}}$	$\sqrt{V^{\mathrm{coef}}_{\mathrm{BLUE}}\{\hat{e}\}}$	$\sqrt{V\{\hat{e}\}}$
BLUE full	0.7739	0.2540	−0.3048	0.2769	−0.1077	−0.03838	0.9516	4.368		
BLUE bootstrap	0.7744	0.2530	−0.3042	0.2769	−0.07789	−0.03891	0.9397	4.343	0.4607	4.368
SD bootstrap	0.4377	0.03962	0.02032	0.02024	0.5542	0.07896	0.4531			

	PF5										
	B98	VSXC	PBE	OP86	HCTH	a_0[b]	a_1[c]	a_2[d]	$\sqrt{V_{\mathrm{BLUE}}\{\hat{e}\}}$	$\sqrt{V^{\mathrm{coef}}_{\mathrm{BLUE}}\{\hat{e}\}}$	$\sqrt{V\{\hat{e}\}}$
BLUE full	0.8033	0.3293	−0.2333	0.2489	−0.1482	−0.4922	0.08028	1.086	4.3033		
BLUE bootstrap	0.8040	0.3302	−0.2320	0.2481	−0.1502	−0.4571	0.07865	1.074	4.273	0.5102	4.303
SD bootstrap	0.4655	0.04780	0.02550	0.02166	0.04339	0.5646	0.08596	0.4409			

[a] All HLC coefficients and $\sqrt{V\{\hat{e}\}}$ values reported in units of kcal/mol. To facilitate future use, the BLUE bootstrap coefficients, recommended for the PF3 method, are in bold. [b] a_0 = constant term. [c] a_1 = weighted sum of n_β terms for functionals combination (eq 26). [d] a_2 = weighted sum of $n_\alpha - n_\beta$ terms for functionals combination (eq 26).

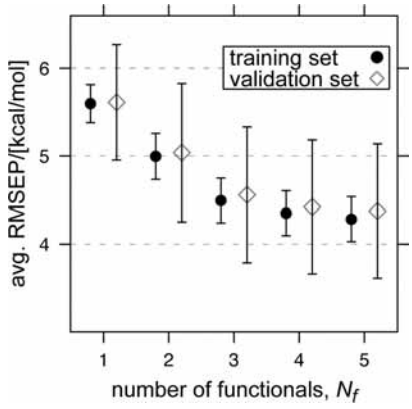

Figure 8. Cross-validation analysis. Mean and standard deviations of training and validation RMSEP for $N_f = 1-5$.

straight line if the data are normally distributed. The residuals of the predicted enthalpies of formation are divided into two sets: G3 molecules, which are known to have small ($\leq \pm 1$ kcal/mol) experimental errors (Figure 9), and the remaining non-G3 molecules (Figure 10). For each set of molecules, we have further subdivided the results to highlight how the best PF combinations perform for certain types of molecules, i.e., hydrocarbons, radicals, first-row molecules, second-row molecules, third-row molecules, fluorinated molecules, and halogenated molecules.

For the G3 set (Figure 9), the molecules with positive residuals (the positive tails) are significantly improved on moving from PF1 to PF3. Little is gained in the overall performance between PF3 and PF5. For all PF levels there is essentially no improvement in the negative tail. Overall, the G3 method performs better than the best PF combination. It is interesting to note that in most cases the shape of the PF probability plots is similar to that of the G3 probability plots, illustrating that their performances are comparable. The G3 and PF3 residuals for both the hydrocarbons and the first- and second-row molecules are straight lines, indicating that they are normally distributed. The radical distribution is also fairly normal, but it is clear from the slopes that the G3 method outperforms the PF method.

For the non-G3 molecules (Figure 10), there is less improvement as the number of functionals in the best PF combination increases. While not as great as for the G3 molecules, there is some visible improvement for the hydrocarbons, first-row molecules, and fluorinated molecules moving from PF1 to PF3. Note the difference in scales for the G3 probability plots (Figure 9) and the non-G3 probability plots (Figure 10), indicating wider error distributions for the non-G3 molecules. This is likely due to the fact that the experimental values for the non-G3 molecules are not known to the same accuracy as the G3 molecules, though we see no evidence of any overall bias in the non-G3 values.

3.7. Bootstrap and Prediction Error. The BLUE optimal weights and prediction error formulas assume that the covariance

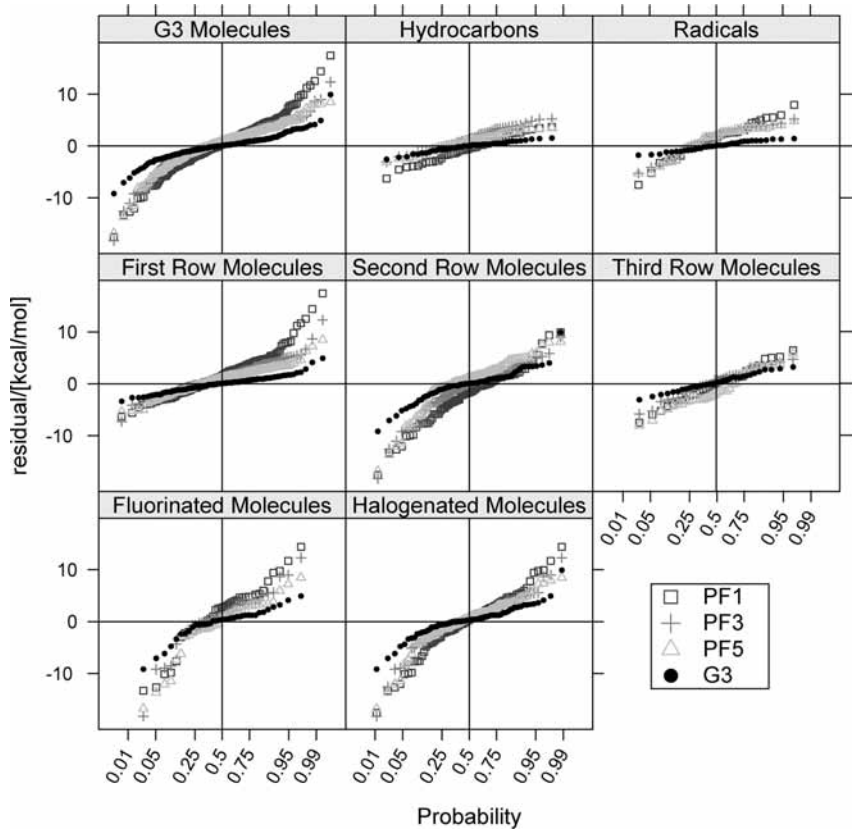

Figure 9. Probability plots of residuals for the G3 molecules using the G3, PF1, PF3, and PF5 methods. The performance of all G3 molecules is illustrated in the upper left panel. All other panels highlight the performance of subsets of molecules as identified by their titles.

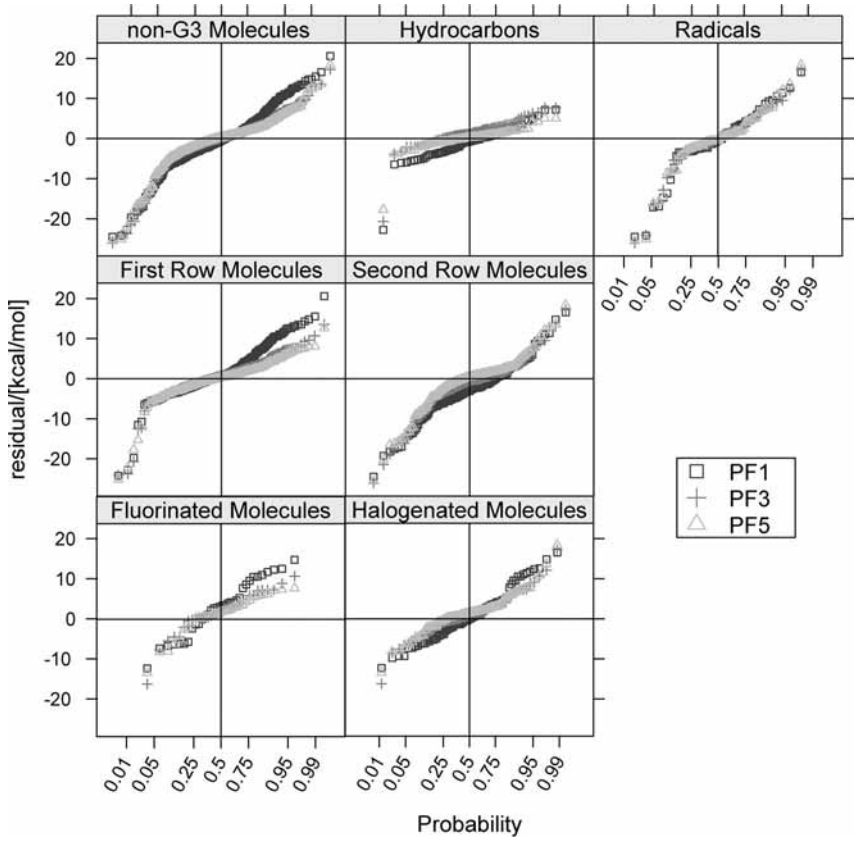

Figure 10. Probability plots of residuals for the non-G3 molecules using the PF1, PF3, and PF5 methods. The performance of all non-G3 molecules is illustrated in the upper left panel. All other panels highlight the performance of molecule subsets as identified by their titles.

matrix of the residuals, $\mathbf{\Sigma}$, is known without error. However, since $\mathbf{\Sigma}$ is estimated from the residuals $e_i(M_k)$ (eq 22), it is subject to sampling fluctuations. This is also true for the parameters in the HLC (eq 6). Therefore, in order to properly

TABLE 3: Comparison of B3LYP, B3LYP w/HLC, PF3, PF5, and G3 Method Prediction Errors for the 271 G3 Molecules, 404 Non-G3 Molecules, and the Full 675 Molecule Data Set Used in the Present Work

method	data set	mean (kcal/mol)	median (kcal/mol)	MAD (kcal/mol)	rms (kcal/mol)
B3LYP	G3	−3.41	−2.18	4.85	6.70
	non-G3	−4.88	−5.19	6.95	8.58
	full set	−4.29	−3.91	6.11	7.89
B3LYP w/HLC	G3	0.30	0.43	3.26	4.41
	non-G3	−0.22	−0.46	4.51	6.27
	full set	−0.01	−0.07	4.01	5.60
PF3	G3	0.45	0.74	2.44	3.37
	non-G3	−0.32	0.12	3.29	5.13
	full set	−0.0082	0.43	2.95	4.51
PF5	G3	0.36	0.83	2.43	3.32
	non-G3	−0.25	0.32	3.03	4.85
	full set	−0.0069	0.46	2.79	4.30
G3	G3	−0.042	0.00	1.18	1.79

estimate the prediction error, the uncertainty in the weights and HLC need to be determined.

To determine these errors, the bootstrap resampling method is used.[68] A random sample with replacement of size 675 is selected from the 675 molecule data set, and the HLC and BLUE estimates are calculated. This is repeated 1000 times and the means and covariance matrix are calculated for the resulting weights and HLC coefficients.

The final coefficients for the functionals included in the PF combination for $N_f = 1-5$ as determined from bootstrapping resampling are in Table 2. Also included are the HLC coefficients for the n_β and $n_\alpha - n_\beta$ terms and the constant term. The coefficients are labeled "BLUE bootstrap". In addition to determining the uncertainty of the BLUE weights and HLC parameters, the bootstrap resampling method is also useful in removing any bias from the estimation equations.[68] The results in Table 2 display no significant bias since the full and bootstrapped coefficients are virtually identical.

The RMSEP $\sqrt{V_{\mathrm{BLUE}}\{\hat{e}\}}$ (eq 13) for both the BLUE full and BLUE bootstrapped methods are reported in Table 2. The variance associated with the uncertainty in the coefficients, evaluated using the bootstrap method, is

$$V_{\mathrm{BLUE}}^{\mathrm{coef}}\{\hat{e}\} = \boldsymbol{\theta}^{\mathrm{T}}\boldsymbol{\Sigma}_{\theta}\boldsymbol{\theta} \tag{27}$$

where $\boldsymbol{\theta} = [w_1,...w_{N_f},a_0,a_1,a_2]^{\mathbf{T}}$, is the row vector of estimated parameters, and $\boldsymbol{\Sigma}_\theta$ is the bootstrap estimated covariance matrix. The $\sqrt{V_{\mathrm{BLUE}}^{\mathrm{coef}}\{\hat{e}\}}$ values are reported in Table 2. Thus, the actual predicted variance for the BLUE estimate is

$$V_{\mathrm{BLUE}}^{\mathrm{total}}\{\hat{e}\} = V_{\mathrm{BLUE}}\{\hat{e}\} + V_{\mathrm{BLUE}}^{\mathrm{coef}}\{\hat{e}\} \tag{28}$$

From Table 2 it is clear that the values of $\sqrt{V_{\mathrm{BLUE}}^{\mathrm{coef}}\{\hat{e}\}}$ for each of the PF levels are insignificant and not required for an accurate estimate of the overall prediction error, $\sqrt{V_{\mathrm{BLUE}}^{\mathrm{total}}\{\hat{e}\}}$. This is a consequence of the large (675 molecule) data set.

It remains to check whether the predicted error variance, $V_{\mathrm{BLUE}}^{\mathrm{total}}\{\hat{e}\}$, for each PF method is correct. For PF1−PF5 the actual variance of $\hat{e}$, $V\{\hat{e}\}$, was determined from the distribution of $\hat{e}(M_k)$ values, where $\hat{e}(M_k)$ is the residual of optimal estimate $\hat{H}$ for a given molecule M_k in the 675 molecule data set. The values of $\sqrt{V\{\hat{e}\}}$ are reported in Table 2. The good agreement with $\sqrt{V_{\mathrm{BLUE}}\{\hat{e}\}}$ illustrates that we are able to make accurate predictions of the error associated with the PF estimate and reinforces the conclusion that the variance associated with the uncertainty in the coefficients $\sqrt{V_{\mathrm{BLUE}}^{\mathrm{coef}}\{\hat{e}\}}$ is insignificant.

3.8. Statistical Summary. Table 3 lists the mean, median, MAD, and rms values for B3LYP, PF3, PF5, and G3. In each column the data is divided into the G3 and non-G3 molecules so that a direct comparison can be made to the G3 method. While there is a severe negative bias in B3LYP, the HLC term in the G3 and PF methods force these distributions to be centered around 0. It is clear that a significant improvement is made moving from the single B3LYP functional to the PF3 method, reducing the MAD and rms by 50%. Comparing the PF3 and PF5 methods, the accuracy of the G3 molecules is the same for both PF combinations, while there is a slight improvement in the accuracy of the non-G3 molecules with the inclusion of two more functionals for PF5. Weighing both the accuracy and computational cost of all the PF combinations, we have identified the PF3 method as the optimal choice. The BLUE bootstrap coefficients for PF3 (bolded in Table 2) are also preferred by the authors, as the bootstrap method removes errors due to bias. To facilitate future use of the PF3 method, we have composed a Perl postprocessing script that extracts information from the required Gaussian 03 output files and computes the enthalpy of formation for a given molecule as estimated by PF3. The text for this program can be found in Supporting Information and may be downloaded from the link provided therein.

Figure 11 emphasizes the accuracy to computational cost relationship for the B3LYP, PF3, and G3 methods. Between each method we see that the MAD is reduced by ∼50% for both the G3 molecule set (diamond) and the full 675 molecule set (asterisk). It is rare to apply G3 to systems with >10−12 atoms but routine to apply DFT methods to significantly larger systems. Therefore, while the G3 method does remain superior to the PF3 method in terms of accuracy, the reduced computational cost for the PF3 method allows for its application on much larger systems.

4. Conclusions

Statistical distributions of the errors in enthalpy of formation as predicted by 18 different density functionals have been analyzed for a test set of 675 molecules. We have identified systematic errors in the predictions of some functionals that depend on the number of valence electrons in the system. Removing this bias reduces the MAD of the best single functional, B3LYP, from 6.12 to 4.02 kcal/mol for the 675 molecule data set. Linear combinations of the unbiased functional estimates can be chosen to exploit correlations among the error distributions and reduce the prediction error. The best combinations of three and five functionals (denoted PF3 and PF5) have MADs of 2.95 and 2.79 kcal/mol, respectively. Including more than five functionals does not significantly improve the accuracy of the predicted enthalpies of formation.

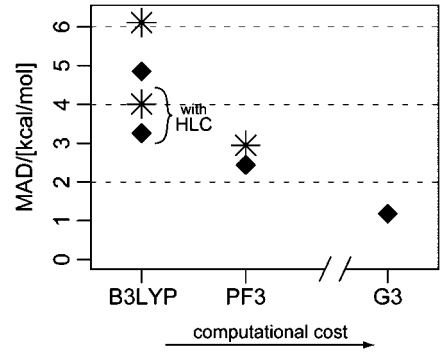

Figure 11. Comparison of MAD values for B3LYP, B3LYP w/HLC, PF3, and G3 methods. Position on the horizontal axis represents the approximate increase in CPU time with respect to a single density functional, B3LYP. ◆, G3 molecule set; *, 675 molecule set.

We recommend the PF3 method, which combines the B3LYP, BLYP, and VSXC functionals. The PF3 method has half the MAD associated with B3LYP, at less than 3 times the computational cost. While the MAD of PF3 is twice that of the widely used G3 method, the cost of G3 is much greater. Thus, PF3 provides reasonable accuracy while still being useful for larger systems or where computational resources are limited.

While PF3 is not as accurate as G3, it is likely that these errors can be improved. As the G*n* methods have evolved, the errors have been reduced by including spin−orbit effects for the atoms and separate HLCs for atoms and open shell molecules. Applying the same approach with PF methods should yield similar improvements. There may also be opportunities to improve the speed or accuracy of PF calculations by using basis set corrections, similar to G*n*, or basis set extrapolation methods. Note that none of these improvements require better functionals, just as the G*n* methods all use the same correlated methods. However, as new functionals are developed, it will be worthwhile to explore whether they can be utilized in PF combinations to further reduce error.

Our analysis has implications for the future development of density functional theory. The systematic bias in the dependence of the prediction error on the number of valence electrons for some commonly used functionals should be assessed in developing new functionals. We have taken a purely empirical approach to correcting for this error and to finding combinations of functionals with improved predictive value. However, since linear combinations of a few functionals can make much more accurate predictions than any individual functional, it appears that forms similar to those used here still have potential for greater accuracy. While other classes of functionals can have their own advantages, relatively simple improvements to commonly used functionals may suffice to achieve chemical accuracy.

Acknowledgment. This research was supported by the National Institute of Environmental Health Sciences through a Superfund Basic Research Program Grant (5RO1ESO15444) and the U.S. Department of Energy under Grant No. DE-FG02-07-ER15921.

Supporting Information Available: Tables S1 and S2, which report BLUE and HLC parameters for all 18 functionals, and an example calculation of the complete PF3 method for isobutene (Table S3 and Scheme S1). This material is available free of charge via the Internet at http://pubs.acs.org. The PF3 program text (Perl postprocessing script) is also available at http://www.ce.udel.edu/faculty/ditoro/.

References and Notes

(1) Bartlett, R. J.; Purvis, G. D *Int. J. Quantum Chem.* **1978**, *14*, 516.
(2) Pople, J. A.; Krishnan, R.; Schlegel, H. B.; Binkley, J. S. *Int. J. Quantum Chem.* **1978**, *14*, 545.
(3) Scuseria, G. E.; Janssen, C. L.; Schaefer, H. F., III *J. Chem. Phys.* **1988**, *89*, 7382.
(4) Scuseria, G. E.; Schaefer, H. F., III *J. Chem. Phys.* **1989**, *90*, 3700.
(5) Cizek, J. *Adv. Chem. Phys.* **1969**, *14*, 35.
(6) Helgaker, T.; Rude, T. A.; Jorgensen, P.; Olsen, J.; Klopper, W. *J. Phys. Org. Chem.* **2004**, *17*, 913.
(7) Klopper, W.; Bak, K. L.; Jorgensen, P.; Olsen, J.; Helgaker, T. *J. Phys. B: At. Mol. Opt. Phys.* **1999**, *23*, R103.
(8) Martin, J. M. L.; Oliveira, D. *J. Chem. Phys.* **1999**, *111*, 1843.
(9) Parthiban, S.; Martin, J. M. L. *J. Chem. Phys.* **2001**, *114*, 6014.
(10) Boese, A. D.; Oren, M.; Atasoylu, O.; Martin, J. M. L.; Kallay, M.; Gauss, J. *J. Chem. Phys.* **2004**, *120*, 4129.
(11) Karton, A.; Rabinovich, E.; Martin, J. M. L. *J. Chem. Phys.* **2006**, *125*, 144108.
(12) Tajti, A.; Szalay, P. G.; Csaszar, A. G.; M, K.; Gauss, J.; Valeev, E.; Flowers, B.; Vazquez, J.; Stanton, J. F. *J. Chem. Phys.* **2004**, *121*, 11599.
(13) Curtiss, L. A.; Jones, C.; Trucks, G. W.; Raghavachari, K.; Pople, J. A. *J. Chem. Phys.* **1990**, *93*, 2537.
(14) Curtiss, L. A.; Raghavachari, K.; Redfern, P. C.; Pople, J. A. *J. Chem. Phys.* **1997**, *106*, 1063.
(15) Raghavachari, K.; Stefanov, B. B.; Curtiss, L. A. *J. Chem. Phys.* **1997**, *106*, 6764.
(16) Baboul, A. G.; Curtiss, L. A.; Redfern, P. C. *J. Chem. Phys.* **1999**, *110*, 7650.
(17) Curtiss, L. A.; Raghavachari, K.; Redfern, P. C.; Pople, J. A. *J. Chem. Phys.* **2000**, *112*, 7374.
(18) Curtiss, L. A.; Raghavachari, K.; Redfern, P. C.; Kedziora, G. S.; Pople, J. A. *J. Phys. Chem. A* **2001**, *105*, 227.
(19) Curtiss, L. A.; Redfern, P. C.; Raghavachari, K. *J. Chem. Phys.* **2005**, *123*, 124107.
(20) Curtiss, L. A.; Redfern, P. C.; Raghavachari, K. *J. Chem. Phys.* **2007**, *126*, 084108.
(21) Petersson, G. A.; Al-Laham, M. A. *J. Chem. Phys.* **1991**, *94*, 6081.
(22) Petersson, G. A.; Tensfeldt, T. G., Jr. *J. Chem. Phys.* **1991**, *94*, 6091.
(23) Montgomery, J. A., Jr. ; Ochterski, J. W.; Petersson, G. A. *J. Chem. Phys.* **1994**, *101*, 5900.
(24) Ochterski, J. W.; Petersson, G. A., Jr. *J. Chem. Phys.* **1996**, *104*, 2598.
(25) J, A; Montgomery, J.; Frisch, M. J.; Ochterski, J. W.; Petersson, G. A. *J. Chem. Phys.* **1999**, *110*, 2822.
(26) Montgomery, J. A., Jr.; Frisch, M. J.; Ochterski, J. W.; Petersson, G. A. *J. Chem. Phys.* **2000**, *112*, 6532.
(27) Cioslowski, J.; Schimeczek, M.; Liu, G.; Stoyanov, V. *J. Chem. Phys.* **2000**, *113*, 9377.
(28) Friesner, R. A.; Murphy, R. B.; Beachy, M. D.; Ringnalda, M. N.; Pollard, W. T.; Dunietz, B. D.; Cao, Y. *J. Phys. Chem. A* **1999**, *103*, 1913.
(29) Kone, M.; Illien, B.; Graton, J.; Laurence, C. *J. Phys. Chem. A* **2005**, *209*, 11907.
(30) Csonka, G. I.; Ruzsinszky, A.; Tao, J.; Perdew, J. P. *Int. J. Quantum Chem.* **2005**, *101*, 506.
(31) Zhao, Y.; Truhlar, D. G. *J. Chem. Theory Compt.* **2005**, *1*, 415.
(32) Friesner, R. A.; Knoll, E. H.; Cao, Y. *J. Chem. Phys.* **2006**, *125*, 124107.
(33) van Voorhis, T.; Scuseria, G. E. *J. Chem. Phys.* **1998**, *109*, 400.
(34) Vydrov, O. A.; Scuseria, G. E. *J. Chem. Phys.* **2004**, *121*, 8187.
(35) Perdew, J. P.; Burke, K.; Ernzerhof, M. *Phys. Rev. Lett.* **1996**, *77*, 3865.
(36) Becke, A. D. *J. Chem. Phys.* **1993**, *98*, 5648.
(37) Seminario, J. M.; Maffei, M. G.; Agapito, L. A.; Salazar, P. F. *J. Phys. Chem. A* **2006**, *110*, 1060.
(38) Fast, P. L.; Corchado, J. C.; Sanchez, M. L.; Truhlar, D. G. *J. Phys. Chem. A* **1999**, *103*, 3139.
(39) Fast, P. L.; Sanchez, M. L.; Corchado, J. C.; Truhlar, D. G. *J. Chem. Phys.* **1999**, *110*, 11679.
(40) Fast, P. L.; Sanchez, M. L.; Truhlar, D. G. *Chem. Phys. Lett.* **1999**, *306*, 407.
(41) Fast, P. L.; Corchado, J. C.; Sanchez, M. L.; Truhlar, D. G. *J. Phys. Chem. A* **1999**, *103*, 5129.
(42) Tratz, C. M.; Fast, P. L.; Truhlar, D. G. *PhysChemComm* **1999**, *2*, 14.
(43) Fast, P. L.; Truhlar, D. G. *J. Phys. Chem. A* **2000**, *104*, 6111.
(44) Lynch, B. J.; Truhlar, D. G. *J. Phys. Chem. A* **2003**, *107*, 3898.
(45) Zhao, Y.; Lynch, B. J.; Truhlar, D. G. *J. Phys. Chem. A* **2004**, *108*, 4786.
(46) *National Institute of Standard and Technology Chemistry Webbook*; U.S. Secretary of Commerce on behalf of the United States of America: Washington, DC, 2005.
(47) Frisch, M. J.; Trucks, G. W.; Schlegel, H. B.; Scuseria, G. E.; Robb, M. A.; *Gaussian 03, Revision B.05*; Gaussian, Inc.: Wallingford, CT, 2004.
(48) Perdew, J. P.; Chevary, J. A.; Vosko, S. H.; Jackson, K. A.; Pederson, M. R.; Singh, D. J.; Fiolhais, C. *Phys. Rev. B* **1992**, *46*, 6671.
(49) Perdew, J. P.; Chevary, J. A.; Vosko, S. H.; Jackson, K. A.; Pederson, M. R.; Singh, D. J.; Fiolhais, C. *Phys. Rev. B* **1993**, *48*, 4978.
(50) Perdew, J. P.; Burke, K.; Wang, Y. *Phys. Rev. B* **1996**, *54*, 16533.
(51) Becke, A. D. *J. Chem. Phys.* **1997**, *107*, 8554.
(52) Schmider, H. L.; Becke, A. D. *J. Chem. Phys.* **1998**, *108*, 9624.
(53) Wilson, P. J.; Bradley, T. J.; Tozer, D. J. *J. Chem. Phys.* **2001**, *115*, 9233.
(54) Becke, A. D. *Phys. Rev. A* **1988**, *38*, 3098.
(55) Lee, C.; Yang, W.; Parr, R. G. *Phys. Rev. B* **1988**, *37*, 785.
(56) Miehlich, B.; Savin, A.; Stoll, H.; Preuss, H. *Chem. Phys. Lett.* **1989**, *157*, 200.
(57) Perdew, J. P. *Phys. Rev. B* **1986**, *33*, 8822.
(58) Vosko, S. H.; Wilk, L.; Nusair, M. *Can. J. Phys* **1980**, *58*, 1200.
(59) Hamprecht, F. A.; Cohen, A. J.; Tozer, D. J.; Handy, N. C. *J. Chem. Phys.* **1998**, *109*, 6264.
(60) Adamo, C.; Barone, V. *J. Chem. Phys.* **1998**, 108.
(61) Handy, N. C.; Cohen, A. J. *Mol. Phys.* **2001**, *99*, 403.

(62) Perdew, J. P.; Burke, K.; Ernzerhof, M. *Phys. Rev. Lett.* **1997**, *78*, 1396.

(63) *NIST-JANAF Thermochemical Tables*, 4th ed.; American Chemical Society and American Institute of Physics for the National Institute of Standards and Technology: Gaithersburg, MD, 1998.

(64) R Development Core Team. *R: A Language and Environment for Statistical Computing*; R Foundation for Statistical Computing: Vienna, Austria, 2007.

(65) Tukey, J. W. *Exploratory Data Analysis*; Addison-Wesley Pub. Co.: Reading, MA, 1977.

(66) Kay, S. M. *Fundamentals of Statistical Signal Processing: Estimation Theory*; Prentice Hall PTR: Upper Saddle River, NJ, 1993.

(67) Aitchison, J.; Brown, J. A. C. *The Lognormal Distribution*; Cambridge University Press: Cambridge, 1957.

(68) Efron, B. *The Jackknife, the Bootstrap and Other Resampling Plans*; Capital City Press: Montpelier, VT, 1982.

JP804784S